A&A 518, L14 (2010)
DOI: 10.1051/0004-6361/201014681

Herschel: the first science highlights

Astronomy & Astrophysics
Special feature

Letter to the Editor

Deep *Herschel* view of obscured star formation in the Bullet cluster⋆

T. D. Rawle[1], S. M. Chung[2], D. Fadda[3], M. Rex[1], E. Egami[1], P. G. Pérez-González[4,1], B. Altieri[5], A. W. Blain[6], C. R. Bridge[6], A. K. Fiedler[1], A. H. Gonzalez[2], M. J. Pereira[1], J. Richard[7], I. Smail[7], I. Valtchanov[5], M. Zemcov[6,8], P. N. Appleton[3], J. J. Bock[6,8], F. Boone[9,11], B. Clement[10], F. Combes[11], C. D. Dowell[6,8], M. Dessauges-Zavadsky[12], O. Ilbert[10], R. J. Ivison[13,14], M. Jauzac[10], J.-P. Kneib[10], D. Lutz[15], R. Pelló[9], G. H. Rieke[1], G. Rodighiero[16], D. Schaerer[12,9], G. P. Smith[17], G. L. Walth[1], P. van der Werf[18], and M. W. Werner[8]

(Affiliations are available in the online edition)

Received 31 March 2010 / Accepted 11 May 2010

ABSTRACT

We use deep, five band (100–500 μm) data from the *Herschel* Lensing Survey (HLS) to fully constrain the obscured star formation rate, $SFR_{\rm FIR}$, of galaxies in the Bullet cluster (z = 0.296), and a smaller background system (z = 0.35) in the same field. *Herschel* detects 23 Bullet cluster members with a total $SFR_{\rm FIR}$ = 144 ± 14 $M_\odot$ yr^{-1}. On average, the background system contains brighter far-infrared (FIR) galaxies, with ~50% higher $SFR_{\rm FIR}$ (21 galaxies; 207 ± 9 $M_\odot$ yr^{-1}). SFRs extrapolated from 24 μm flux via recent templates ($SFR_{24\,\mu\rm m}$) agree well with $SFR_{\rm FIR}$ for ~60% of the cluster galaxies. In the remaining ~40%, $SFR_{24\,\mu\rm m}$ underestimates $SFR_{\rm FIR}$ due to a significant excess in observed S_{100}/S_{24} (rest frame S_{75}/S_{18}) compared to templates of the same FIR luminosity.

Key words. galaxies: clusters: individual: Bullet cluster – galaxies: star formation – infrared: galaxies – submillimeter: galaxies

1. Introduction

In the last decade many studies have attempted to quantify the star formation rate (SFR) within cluster galaxies. Ultraviolet and optical observations have successfully identified trends between unobscured star formation and local environment, suggesting that star formation in cluster core galaxies is generally more quenched (e.g. Kodama et al. 2004; Porter & Raychaudhury 2007). However, star formation can be obscured by dust, which re-emits stellar light in the far-infrared (FIR), peaking at a rest frame $\lambda_0 \sim 100$ μm. Mid-infrared surveys (e.g. Metcalfe et al. 2005; Geach et al. 2006; Fadda et al. 2008) have explored obscured star formation by estimating total FIR luminosity from template spectra. These templates are often based on small numbers of well constrained local galaxies, e.g. Rieke et al. (2009).

The PACS (Poglitsch et al. 2010) and SPIRE (Griffin et al. 2010) instruments, onboard the ESA *Herschel* Space Observatory (Pilbratt et al. 2010), enable unprecedented multiband coverage of the FIR. The *Herschel* Lensing Survey (HLS; PI: E Egami) consists of 5-band observations (100–500 μm) of 40 nearby clusters ($z \sim 0.2$–0.4). Nominally devised to exploit the gravitational lensing effect of massive clusters to observe high redshift galaxies (see Egami et al. 2010, for details on survey design), a useful by-product is deep FIR observations of the clusters themselves. At these redshifts, *Herschel* photometry spans the peak of the dust component, allowing an accurate constraint of far infrared luminosity, $L_{\rm FIR}$, and hence obscured SFR.

During the *Herschel* science demonstration phase, HLS observed the Bullet cluster (1E0657–56; z = 0.296). The reason for this choice was two-fold. First, previous studies report bright submillimeter galaxies in the background (e.g. Rex et al. 2009), with HLS analysis presented in Rex et al. (2010). Second, the Bullet cluster is a recent collision of two clusters (Markevitch et al. 2002), offering a unique laboratory for the study of star formation within a dynamic environment. The sub-cluster has conveniently fallen through the main cluster perpendicular to the line of sight (<8° from the sky plane; Markevitch et al. 2004). Analysis of X-ray emission shows that a supersonic bow shock precedes the hot gas, while the weak lensing mass profile indicates that this X-ray bright component lags behind the sub-cluster galaxies due to ram pressure (Markevitch et al. 2002; Barrena et al. 2002). A recent mid-infrared study by Chung et al. (2009) concluded that ram pressure from the merger event had no significant impact on the star formation rates of nearby galaxies. We can re-evaluate these previous studies by using *Herschel* data to constrain $L_{\rm FIR}$ directly. In this letter, we present an exploration of obscured star formation in this cluster environment.

2. Observations

2.1. Photometric data

Five band *Herschel* imaging was obtained using two instruments: PACS (100 160 μm) covering approximately 8′ × 8′ and SPIRE (250 350 500 μm) with a wider ~17′ × 17′ field. We also use Magellan IMACS optical, *Spitzer* IRAC and MIPS 24 μm

⋆ *Herschel* is an ESA space observatory with science instruments provided by European-led Principal Investigator consortia and with important participation from NASA. Data presented in this paper were analyzed using "The *Herschel* Interactive Processing Environment (HIPE)", a joint development by the *Herschel* Science Ground Segment Consortium, consisting of ESA, the NASA *Herschel* Science Center, and the HIFI, PACS and SPIRE consortia.

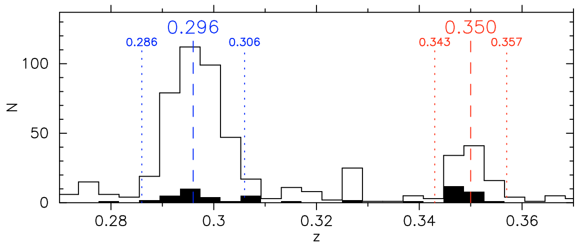

Fig. 1. Distribution of spectroscopic redshifts ($0.27 < z < 0.37$) for galaxies within the Bullet cluster field (outline). *Herschel* detected galaxies are also shown (filled). In addition to the Bullet cluster (z = 0.296), there is a background system at z = 0.350. Dotted lines show our membership limits of 3000 km s^{-1} and 2000 km s^{-1} respectively.

maps with similar coverage to SPIRE, and high resolution *HST* ACS images of the central 4′ × 4′. Egami et al. (2010) provides details of all the data, and presents *Herschel* FIR maps.

The deep SPIRE maps have detection limits well below the instrument confusion limits. To avoid compiling sourcelists from confused maps, *Herschel* fluxes are measured at all *Spitzer* MIPS 24 μm source positions. For a typical galaxy SED at $z \sim 0.3$, the 24 μm map is much deeper than SPIRE, so even with a relatively high $S/N > 10$ cut (flux limit ~100 μJy), we can assume the inclusion of all sources contributing significant FIR flux. The use of mid-infrared source positions has the added advantage of decreasing the significance of flux boosting, which has not been addressed in this study.

Photometric analysis followed the same procedure in all 5 *Herschel* bands. An average PSF, measured from the brightest unblended sources in the image, was simultaneously fit to all positions in the 24 μm catalogue (without re-centering) using DAOPHOT ALLSTAR. At the longer SPIRE wavelengths, there is a higher probability of more than one 24 μm source falling within the FIR beam. In these instances, the objects are grouped together at the 24 μm S/N-weighted mean position, treated as a single source, and flagged (see following sub-section). For more details on the photometry technique see Rex et al. (2010).

2.2. Spectroscopy and sample selection

The spectroscopic redshift catalogue combines observations from three campaigns: Magellan IMACS multi-slit (856 targets, Chung et al. 2010, Chung et al. in prep.), CTIO Hydra multi-fiber (202, Fadda et al. in prep.) and VLT FORS multi-slit (14, J. Richard, private communication). Egami et al. (2010) provides further details. The merged catalogue comprises 929 sources within the SPIRE field.

Figure 1 presents the distribution of spectroscopic redshifts for the range $0.27 < z < 0.37$. An important aspect of this study is confidence in the cluster membership of galaxies. The Bullet cluster distribution peaks at z = 0.296, and we limit membership to ±3000 km s^{-1} ($0.286 < z < 0.306$). In addition, this study also analyzes galaxies from a system at z = 0.350 in the same field, limiting membership to ±2000 km s^{-1} ($0.343 < z < 0.357$). The systems have 362 and 95 known members respectively.

The sample for this analysis consists of MIPS 24 μm sources with spectroscopically confirmed cluster redshifts. These two catalogues were merged by identifying the closest 24 μm source, within the rms pointing error of MIPS (1.4″), to the spectroscopic position. For sample members grouped during the FIR photometry (previous sub-section), we examined the optical and IRAC colours of each group member, identifying the likely source of the mid- and far-IR flux. In cases where the sample member was not considered to be the source, or when the situation was unclear, the object was rejected from the sample.

In the final sample, there are 47 confirmed Bullet cluster members, and an additional 28 sources in the z = 0.35 system. Of these, 23 and 21 galaxies respectively are detected in the *Herschel* bands, highlighted by the filled distribution in Fig. 1. The background system has a much higher fraction of *Herschel* detections than the Bullet cluster (75% of 24 μm sources, compared to 50%).

3. Results and discussion

3.1. Far-infrared (FIR) spectral energy distributions

For each source, the FIR spectral energy distribution (SED) is fit to all available *Herschel* data points, taking into account the upper limits for non-detections. The dust component is modeled by a modified, single-temperature, blackbody

$$S_\nu = N(\nu/\nu_0)^\beta B_\nu(T) \quad (1)$$

where S_ν is flux density, β is dust emissivity index (fixed at 1.5; using β = 2.0 would vary $L_{\rm FIR}$ by <15% on average) and $B_\nu(T)$ is the Planck blackbody radiation function for a source at temperature T. The shape of this optically thin (rather than thick) blackbody imitates the inclusion of a secondary (warm) dust component. As we are concerned only with $L_{\rm FIR}$ and SFR, the parameterization of the data is the most important aspect, and T is used purely as a fit parameter. Galaxies within the PACS field have well constrained fits, and T is allowed to float freely. For those without PACS data (~40%), T_0 has been forced to a narrow range centered on the mean value from the constrained SEDs (30 ± 1 K). Forcing T_0 to a similarly narrow range about values ~1σ from the constrained mean, varies $L_{\rm FIR}$ by <25%. Bias in $L_{\rm FIR}$ due to model priors is comparable in scale to systematics from instrument calibration.

$L_{\rm FIR}$ is integrated over (rest frame) λ_0 = 8–1000 μm from which $SFR_{\rm FIR}$ is derived using the Kennicutt (1998) relation. As an illustration, Fig. 2 displays the FIR SED fits for five of the most luminous galaxies in the sample. These simple fits may underestimate $L_{\rm FIR}$ by up to a factor of 1.8 (Rex et al. 2010), as they lack a mid-infrared component. Future analysis will fully account for additional components. For the purposes of this study, a blackbody fit is sufficient. The luminosities of galaxies in the background system have been de-magnified using the Bullet cluster lensing model of Paraficz et al. (in prep.). The remaining figures in this paper present de-magnified values.

3.2. Star formation rates within the systems

The system at z = 0.35 contains IR galaxies brighter than those in the Bullet cluster, with three galaxies meeting the LIRG criterion [$\log(L_{\rm FIR}/L_\odot) \gtrsim 11.0$] and an additional two within 1σ. A further 10 members have $\log(L_{\rm FIR}/L_\odot) > 10.5$. In contrast, the Bullet cluster contains two LIRGs, and only six other galaxies brighter than $\log(L_{\rm FIR}/L_\odot) = 10.5$.

The total star formation rate of the 23 Bullet cluster galaxies is 144 ± 14 $M_\odot$ yr^{-1}. The 21 galaxies in the background system are, on average, ~50% more active, with a total SFR = 207 ± 9 $M_\odot$ yr^{-1}. Only five of these galaxies have been magnified by more than 20%, and the minimum detected SFRs are similar in each system. Therefore, it is unlikely that the higher total SFR is due to a decreased lower limit caused by magnification. The difference is likely to reflect the mass of the systems, although the lower SFR in the Bullet cluster may indicate that cluster-cluster mergers are not important for triggering FIR starbursts.

Figure 3 displays the spatial distribution of the *Herschel*-derived SFR for the two systems. Flux densities in optical

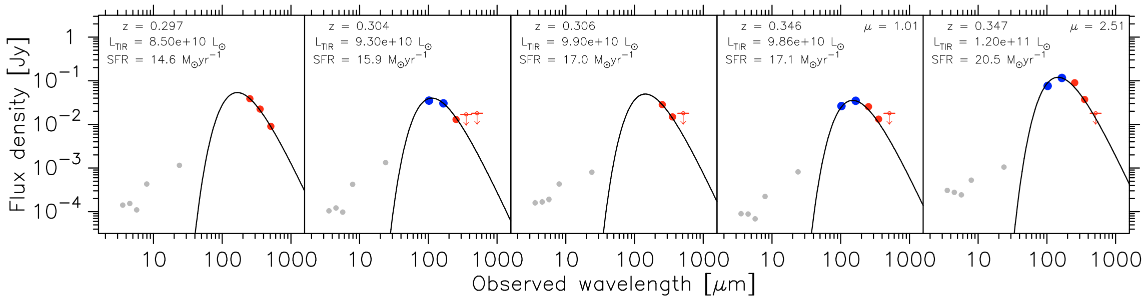

Fig. 2. Photometric data for five of the most FIR luminous galaxies in the sample. Blue = PACS; red = SPIRE; grey = IRAC/MIPS. Flux densities are as observed (i.e. not de-magnified). Redshift and, for background system galaxies, magnification factor, μ, are displayed at the top of each panel. L_{FIR} and SFR_{FIR} derived from the best fit blackbody (black line) are also shown and have been de-magnified where necessary.

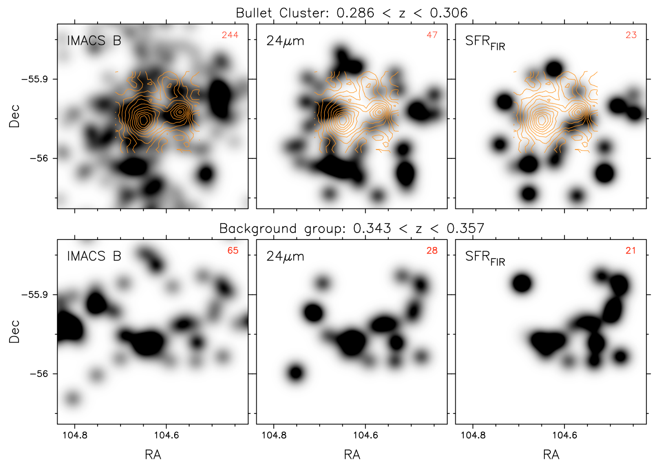

Fig. 3. Smoothed density maps for IMACS B-band flux (*left panels*), 24 μm flux (*central*) and SFR calculated from *Herschel* data (*right*). The sources are binned by confirmed system membership, with the number of contributing galaxies displayed in the *upper-right* of each panel: *upper row* for Bullet cluster (over-plot in orange by the weak lens mass map); lower row for $z = 0.35$ system. All maps are Gaussian smoothed to the SPIRE 250 μm beam size (18″ *FWHM*).

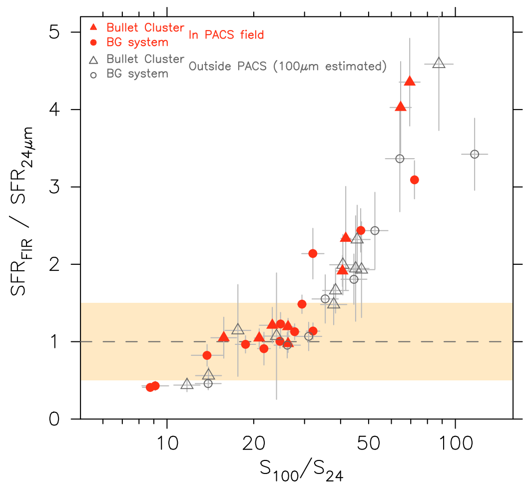

Fig. 4. Ratio of SFR_{FIR} (from blackbody fit) to $SFR_{24\,\mu\mathrm{m}}$ (via Rieke et al. 2009) versus the flux ratio S_{100}/S_{24}. For galaxies outside the PACS field, 100 μm is predicted from the blackbody fit. Dashed line is equality and shaded region indicates 50% difference in the SFRs. All galaxies with under-predicted $SFR_{24\,\mu\mathrm{m}}$ have redder S_{100}/S_{24}.

B-band and 24 μm are shown for comparison. An initial examination suggests that the Bullet cluster exhibits a radial trend in SFR_{FIR} (lacking significant FIR detection towards the centre), reminiscent of that found in other contemporary studies (Braglia et al. 2010; Pereira et al. 2010). The gradient in the Bullet cluster SFR is examined in detail in Chung et al. (in prep.).

The IR and optical flux of the background system trace similar distributions, whereas in the Bullet cluster, the B-band flux is more centrally concentrated, away from the IR sources. This may indicate a different trend in dust retention for the two systems. While the 24 μm and *Herschel* SFR density maps generally trace the same distribution, there are significant outliers: bright 24 μm sources with relatively lower SFRs, and vice versa. In the following section, we compare the SFR estimated from 24 μm (through the Rieke et al. 2009, templates) to the SFR_{FIR}.

3.3. 24 μm as a L_{FIR} predictor in nearby clusters

The mid-infrared bands, e.g. MIPS 24 μm, are often used to estimate far infrared luminosity, L_{FIR}, and hence obscured SFR, via template FIR SEDs such as Rieke et al. (2009). Those authors provide a simple formula (their Eq. (14)) to convert 24 μm flux directly to SFR. The templates are based on local (U)LIRGs ($z \lesssim 0.1$), and at high redshift, may not be valid. Here, we test the template accuracy for cluster galaxies at $z = 0.3$.

In Sect. 3.2 (Fig. 3), we suggested that while 24 μm flux and SFR_{FIR} follow the same general distribution, they are not perfectly correlated. A direct comparison of SFR_{FIR} to $SFR_{24\,\mu\mathrm{m}}$ (Fig. 4; plotted against the dust-peak-mid-IR flux ratio) leads to the same conclusion. For ~60% of galaxies, the two SFRs agree well. However, there are several galaxies (~30%) that have severely underestimated $SFR_{24\,\mu\mathrm{m}}$, and these also display systematically redder S_{100}/S_{24}. If SFR_{FIR} is underestimated by the simple blackbody fits (Sect. 3.1), the $SFR_{24\,\mu\mathrm{m}}$ predictions are correspondingly worse.

Are the under-predicted $SFR_{24\,\mu\mathrm{m}}$ caused by the redder S_{100}/S_{24} colours? Figure 5 examines the Rieke et al. templates more closely, comparing them to the *Herschel* fluxes. For templates spanning the L_{FIR} range of the observations, the agreement is good for $\lambda_0 \gtrsim 200$ μm. However, at 100 μm there are 8 significant outliers; we define 100 μm excess galaxies as those with S_{100}/S_{24} (rest frame S_{75}/S_{18}) > 30 as the templates predict $S_{100}/S_{24} \lesssim 20$. Only templates with very high luminosities, i.e. $\log(L_{\mathrm{FIR}}/L_{\odot}) \geq 12$, match the observed S_{100}/S_{24}, but even the brightest sample galaxy has only $\log(L_{\mathrm{FIR}}/L_{\odot}) \sim 11.5$, while most are $\log(L_{\mathrm{FIR}}/L_{\odot}) < 11$. Although high L_{FIR} templates have $S_{100}/S_{24} \gtrsim 30$, their lower peak wavelength leads to an under-prediction at $\lambda \gtrsim 200$ μm in at least three observed SEDs. We also compare to the least active Dale & Helou (2002) FIR templates ($\alpha = 1.8{-}2.5$). The locus of these are substantially similar to the low luminosity Rieke et al. templates and thus also only

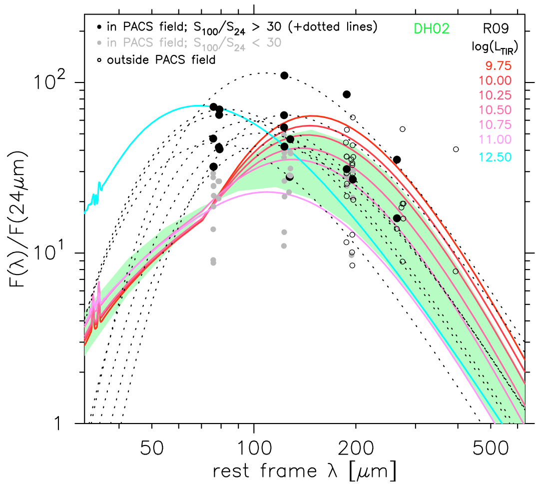

Fig. 5. Observed *Herschel* fluxes normalized by 24 μm for galaxies in both systems. Symbols as described at top-left. Rieke et al. (2009) average templates for $9.75 \leq \log(L_{\rm FIR}) \leq 11.0$ (red-pink) plus one example high-$L_{\rm FIR}$ template (cyan). Locus of low-activity templates from Dale & Helou (2002) (α = 1.8–2.5) is shaded green. All templates are normalized at $\lambda_{\rm obs}$ = 24 μm (λ_0 = 18 μm). Templates in $L_{\rm FIR}$ range of the observations under-predict S_{100}/S_{24} for 40% of sources. High $L_{\rm FIR}$ templates do not match the shape at $\lambda \geq 200$ μm.

under-predict S_{100}/S_{24}. We stress that, unlike $L_{\rm FIR}$ and $SFR_{\rm FIR}$, the presence of a 100 μm excess is independent of the blackbody fits and the systematic uncertainties therein.

Galaxies with a 100 μm excess account for ~40% of cluster members detected with PACS, and cover the entire range of $L_{\rm FIR}$ sampled. Above a nominal luminosity limit of 10^{10} $L_\odot$, 55% of Bullet cluster galaxies have the 100 μm excess. The fraction in the background system is lower at 36%. This may indicate a trend with environment, or could be due to the off-centre view of the latter system (i.e. a potential radial trend). High resolution HST imaging covers five of the eight 100 μm excess galaxies (Fig. 6). Despite the small number, the galaxies span a broad range of types and morphologies. Further examples are required for a firm conclusion, but these suggest that the 100 μm excess is not due to a single population of galaxies.

The S_{100}/S_{24} colours alone may have led to the conclusion that the 100 μm excess was due to galaxies with generally colder dust. However, fits to the combined HLS PACS+SPIRE photometry suggest that this is not the case. Rather, the excess may be due to an additional warm dust component or active galactic nuclei (AGN) which are not considered in the templates. Using a simple power law to parameterize flux in the range 24–100 μm, we estimate the AGN contribution to total bolometric luminosity via the S_{60}/S_{25} indicator for ULIRGs (Veilleux et al. 2009, Fig. 36). None of the 100 μm excess galaxies have predicted AGN fractions >30%. However, we may be under-predicting the contribution if the mid-IR SED steepens beyond 60 μm, or if the indicator breaks down for galaxies in this luminosity range.

Herschel PACS observations of $z \sim 0.2$ LoCuSS clusters (without the advantage of complementary SPIRE data), display a similar fraction of 100 μm excess galaxies (Smith et al. 2010; Pereira et al. 2010). However, the high redshift field sample from the HLS Bullet cluster observations (Rex et al. 2010) lacks a comparable excess at $\lambda_0 \approx 75$ μm. These results suggest that the effect could be either redshift dependent or cluster-specific. HLS

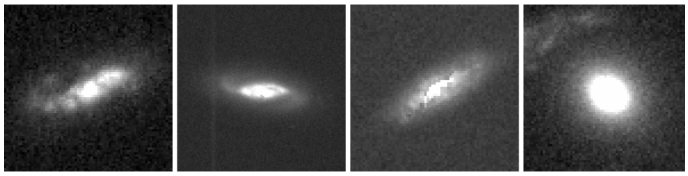

Fig. 6. HST ACS thumbnails of five 100 μm excess galaxies (S_{100}/S_{24} > 30; increasing from left) do not suggest a single source population.

is well placed for further analysis of the S_{100}/S_{24} phenomenon, as the combined PACS+SPIRE data ensures that both the excess and entire FIR component can be constrained simultaneously.

4. Conclusions

Using deep *Herschel* observations (100–500 μm) to fully constrain the FIR component, we derive obscured SFRs for galaxies in the Bullet cluster (z = 0.296), and a background system (z = 0.35) in the same field. *Herschel* detects 23 Bullet cluster members, with a total $SFR_{\rm FIR}$ = 144 ± 14 $M_\odot$ yr^{-1}, while the background system contains 21 detections but ~50% higher SFR (207 ± 9 $M_\odot$ yr^{-1}). The relative distributions of $SFR_{\rm FIR}$ and optical flux suggest a difference in dust retention between the two systems. For ~60% of galaxies, $SFR_{\rm FIR}$ agrees well with estimated SFRs from 24 μm flux via recent templates. However, the remaining galaxies display a significant excess at 100 μm ($\lambda_0 \approx 75$ μm) compared to templates, which causes an under-prediction in $SFR_{24\,\mu{\rm m}}$. We note that such an excess is not found in the high redshift, field sample (Rex et al. 2010). Future studies will exploit the full range of 5-band *Herschel* cluster observations available in HLS, to form a more complete understanding of the environmental effect on obscured star formation rates, and explore the origin and dependencies of the 100 μm excess.

Acknowledgements. This work is based in part on observations made with *Herschel*, a European Space Agency Cornerstone Mission with significant participation by NASA. Support for this work was provided by NASA through an award issued by JPL/Caltech.

References

Barrena, R., Biviano, A., Ramella, M., Falco, E. E., & Seitz, S. 2002, A&A, 386, 816
Braglia, F. G., Ade, P. A. R., Bock, J. J., et al. 2010, MNRAS, submitted [arXiv:1003.2629]
Chung, S. M., Gonzalez, A. H., Clowe, D., et al. 2009, ApJ, 691, 963
Chung, S. M., Gonzalez, A. H., Clowe, D., Markevitch, M., & Zaritsky 2010, ApJ, submitted
Dale, D. A., & Helou, G. 2002, ApJ, 576, 159
Egami, E., et al. 2010, A&A, 518, L12
Fadda, D., Biviano, A., Marleau, F. R., Storrie-Lombardi, L. J., & Durret, F. 2008, ApJ, 672, L9
Geach, J. E., Smail, I., Ellis, R. S., et al. 2006, ApJ, 649, 661
Griffin, M. J., et al. 2010, A&A, 518, L3
Kennicutt, Jr., R. C. 1998, ARA&A, 36, 189
Kodama, T., Balogh, M. L., Smail, I., Bower, R. G., & Nakata, F. 2004, MNRAS, 354, 1103
Markevitch, M., Gonzalez, A. H., Clowe, D., et al. 2004, ApJ, 606, 819
Markevitch, M., Gonzalez, A. H., David, L., et al. 2002, ApJ, 567, L27
Metcalfe, L., Fadda, D., & Biviano, A. 2005, Space Sci. Rev., 119, 425
Pereira, M. J., et al. 2010, A&A, 518, L40
Pilbratt, G. L., et al. 2010, A&A, 518, L1
Poglitsch, A., et al. 2010, A&A, 518, L2
Porter, S. C., & Raychaudhury, S. 2007, MNRAS, 375, 1409
Rex, M., Ade, P. A. R., Aretxaga, I., et al. 2009, ApJ, 703, 348
Rex, M., et al. 2010, A&A, 518, L13
Rieke, G. H., Alonso-Herrero, A., Weiner, B. J., et al. 2009, ApJ, 692, 556
Smith, G. P., et al. 2010, A&A, 518, L18
Veilleux, S., Rupke, D. S. N., Kim, D., et al. 2009, ApJS, 182, 628

Page 5 is available in the electronic edition of the journal at http://www.aanda.org

[1] Steward Observatory, University of Arizona, 933 N. Cherry Ave, Tucson, AZ 85721, USA
e-mail: eegami@as.arizona.edu
[2] Department of Astronomy, University of Florida, Gainesville, 32611-2055, USA
[3] NASA *Herschel* Science Center, California Institute of Technology, MS 100-22, Pasadena, CA 91125, USA
[4] Departamento de Astrofísica, Facultad de CC. Físicas, Universidad Complutense de Madrid, 28040 Madrid, Spain
[5] *Herschel* Science Centre, ESAC, ESA, PO Box 78, Villanueva de la Cañada, 28691 Madrid, Spain
[6] California Institute of Technology, Pasadena, CA 91125, USA
[7] Institute for Computational Cosmology, Department of Physics, Durham University, South Road, Durham DH1 3LE, UK
[8] Jet Propulsion Laboratory, Pasadena, CA 91109, USA
[9] Laboratoire d'Astrophysique de Toulouse-Tarbes, Université de Toulouse, CNRS, 14 Av. Edouard Belin, 31400 Toulouse, France
[10] Laboratoire d'Astrophysique de Marseille, CNRS – Université Aix-Marseille, 38 rue Frédéric Joliot-Curie, 13388 Marseille Cedex 13, France
[11] Observatoire de Paris, LERMA, 61 Av. de l'Observatoire, 75014 Paris, France
[12] Geneva Observatory, University of Geneva, 51 Ch. des Maillettes, 1290 Versoix, Switzerland
[13] UK Astronomy Technology Centre, Science and Technology Facilities Council, Royal Observatory, Blackford Hill, Edinburgh EH9 3HJ, UK
[14] Institute for Astronomy, University of Edinburgh, Blackford Hill, Edinburgh EH9 3HJ, UK
[15] Max-Planck-Institut für extraterrestrische Physik, Postfach 1312, 85741 Garching, Germany
[16] Department of Astronomy, University of Padova, Vicolo dell'Osservatorio 3, 35122 Padova, Italy
[17] School of Physics and Astronomy, University of Birmingham, Edgbaston, Birmingham, B15 2TT, UK
[18] Sterrewacht Leiden, Leiden University, PO Box 9513, 2300 RA Leiden, The Netherlands